Comput Mech
DOI 10.1007/s00466-009-0407-2

ORIGINAL PAPER

Bergström–Boyce model for nonlinear finite rubber viscoelasticity: theoretical aspects and algorithmic treatment for the FE method

Hüsnü Dal · Michael Kaliske

Received: 2 September 2008 / Accepted: 30 June 2009

Abstract One of the successful approaches to model the time-dependent behaviour of elastomers is proposed by Bergström and Boyce (JMPS 46:931–954, 1998). The model is micromechanically inspired from the relaxation of a single entangled chain in a polymer gel matrix. Although the theory of inelasticity based on multiplicative decomposition of the deformation gradient is well established, the complexity of the nonlinear evolution law as well as the nonlinear equilibrium and non-equilibrium material response necessitates a precise description of the algorithmic setting. This contribution presents for the first time a novel numerical implementation of the Bergström–Boyce model in the context of finite element analysis and elaborates theoretical aspects of the model. The thermodynamical consistency of the evolution law is proven and a parameter study with respect to the material parameters has been carried out. The agreement of the model with the recent experimental data is investigated.

Keywords Finite viscoelasticity · Rubber viscoelasticity · Hysteresis · Algorithmic setting · Thermodynamical consistency

1 Introduction

Rubbery polymers exhibit both elastic and viscous material behaviour simultaneously. The non-equilibrium response of rubbery polymers attracted many scientists from applied physics, material science and engineering. Since elastomeric materials constitute a great part in industry, the importance of precise analysis and design necessitates the incorporation of highly sophisticated material models in simulation tools. One of the recent attempts for the description of rate-dependent material behaviour of rubbery polymers is made by Bergström and Boyce [1]. In the contribution on hand, theoretical and numerical aspects of the Bergström and Boyce model (*BB model*) will be discussed. It will be shown that the proposed evolution law is a more general representation of the finite viscoelasticity model of Reese and Govindjee [2], with slight differences. Reese and Govindjee [2] proposed an evolution law which, when linearized around the thermodynamic equilibrium, yields the finite linear viscoelasticity model of Lubliner [3]. Ignoring the volumetric viscosity term in the finite viscoelasticity model and extending the materially linear evolution of Reese and Govindjee [2], one obtains a more general expression for finite viscoelasticity as proposed by Bergström and Boyce [1]. It will be further demonstrated that the algorithmic implementation of the model can be done similarly to the algorithm proposed by Simo and Miehe [4] for finite elastoplasticity and by Simo [5] for viscoplasticity. Integration of the evolution law will be carried out by an exponential mapping algorithm (see Weber and Anand [6], Cuitino and Ortiz [7]). Such an approach has been adopted to finite viscoelasticity by Reese and Govindjee [2]. With slight modifications, the same algorithmic structure can be restructured for the *BB model*. The finite viscoelasticity model proposed by Reese and Govindjee [2] is constructed on the Ogden type material models (see Ogden [8]). However, the algorithm proposed in [2] covers a general framework of viscoelasticity based on a multiplicative split of deformation gradient and an evolution law as a function of elastic left Cauchy-Green tensor $\boldsymbol{b}_e$. The evolution law proposed has a simple linear form which includes a constant volumetric and isochoric viscosity terms. The evolution law of the *BB model* includes invariants of the inelastic right Cauchy-Green tensor $\boldsymbol{C}_i$ which spoils the simple representation in terms of principal stretches of $\boldsymbol{b}_e$

H. Dal · M. Kaliske (✉)
Institute for Structural Analysis, Technische Universität Dresden, 01062 Dresden, Germany
e-mail: michael.kaliske@tu-dresden.de

Published online: 09 August 2009

Recently, Areias and Matous [9] developed a new finite element formulation for viscoelastic materials and employed the method for the *BB model*. The evolution law is rewritten in a Lagrangean setting in terms of rate of $\boldsymbol{C}_i$. The residual expression stemming from the evolution law is updated for $\boldsymbol{C}_i$ and $\Delta\gamma$. We will extend the algorithmic approach adopted by Reese and Govindjee [2] for the implementation of the *BB model* within a distinct framework of volumetric-isochoric split of the free energy density. Within this context, the generalized stresses and the moduli expressions necessary for standard and mixed Jacobian-pressure finite element formulation (Q1/P0 element) will be derived. The advantage of the proposed formulation over the formulation of Areias and Matous [9] is that inversion operations involve only 3×3 matrices with 3 unknowns in the eigenspace of $\boldsymbol{b}_e$, whereas the latter formulation involves lengthy operations with tensor inversions. However, this is done at the expense of accuracy of the algorithm since the invariant terms of $\boldsymbol{C}_i$ in the evolution law are a priori assumed to be constant and updated from the history variables for a given time step.

1.1 Constitutive approaches to rubber elasticity and viscoelasticity

Many material models for the description of the elastic and viscous behaviour of rubber exist. The accuracy of a proposed viscoelasticity model depends not only on the performance of the constitutive law for the evolution of the internal variable, but also on the constitutive model describing the ground state elastic response. Recently, Marckmann and Verron [10] discussed 21 rubber elasticity models and compared the performance of the formulations with respect to the fitting capabilities to uniaxial tension, equibiaxial tension and pure shear data from Treloar [11] and Kawabata et al. [12], according to the fitting capability up to stretch level of 400% at which the isoprene rubber shows a reversible elastic behaviour without crystallization. The extended tube model of Kaliske and Heinrich [13], the micro-sphere model of Miehe et al. [14] and the Ogden model are cited as the most successful models among others. The Ogden model depends on a phenomenological description of the free energy function and the model parameters do not have any physical interpretation. The success of the extended tube model and the micro-sphere model depends on the incorporation of tube like constraints which take into account the restrictions on the motion of a free chain due to the chains in the neighbourhood or the so-called forest chains. Additional to a tube constraint part, the micro-sphere model depends on an average network stretch which is linked to the macro-continuum stretches *via* root averaging of the macro stretches in discrete orientation directions. The *BB model* uses the *8-chain model* of Arruda and Boyce [15] for the ground state elastic response and for the Maxwell branch of the model. The *8-chain model* provides quite satisfactory results for uniaxial data, however, underestimates the equi-biaxial and pure shear response at moderate and large deformations due to the fixed relationship between locking stretches for different deformation modes. On the other hand, considering that the model depends only on two material parameters, it yields quite satisfactory results and the simplicity of the parameter identification makes the model popular for industrial applications.

Two molecular approaches for the description of the time-dependent behaviour of polymers exist. *Transient network theory* explains the stress relaxation phenomenon as a consequence of breakage and reformation of the cross-links constantly. The theory is first proposed by Green and Tobolsky [16] and further developed by Lodge [17], Phan-Thien [18] and Tanaka and Edwards [19,20]. *Reptation-type tube models* are developed for the definition of the motion of a single chain in a polymer gel. The constraints on the free motion of a single chain are qualitatively modeled as a tube-like constraint and the motion of the chain is described as a combination of Brownian motion within and reptational motion along the tube. The model is proposed by De Gennes [21] and Doi and Edwards [22]. The reptational motion is successfully adopted to finite viscoelasticity by Bergström and Boyce [1]. Recently, Miehe and Göktepe [23] proposed a finite viscoelasticity model depending on two micro-kinematic scalar internal variables on discrete space orientations of the micro-sphere. They propose two micro-mechanisms for the relaxation process of polymer chains: The relaxation of superimposed entanglements and the release of topological constraints is taken into account by a-spectrum of nonlinear evolution laws in the logarithmic space of the discrete space orientations.

The paper is organized as follows: In Sect. 2, the basic equations governing finite viscoelasticity and the thermodynamics in terms of the concept of dissipation are introduced. Section 3 presents a complete algorithmic setting for the Bergström–Boyce model suitable for large strain finite element analysis. In Sect. 4, the efficiency of the model is validated with a benchmark example and a parameter study with respect to material parameters is carried out. Finally, concluding remarks close the paper.

2 Continuum mechanical basis of viscoelasticity

Let $\boldsymbol{\varphi} : \boldsymbol{X} \mapsto \boldsymbol{x}$ be the deformation map at time $t \in \mathbb{R}_+$ of a body. $\boldsymbol{\varphi}$ maps points $\boldsymbol{X} \in \mathscr{B}$ of the reference configuration $\mathscr{B} \subset \mathbb{R}^3$ onto points $\boldsymbol{x} = \boldsymbol{\varphi}(\boldsymbol{X}; t) \in \mathscr{S}$ of the current configuration $\mathscr{S} \subset \mathbb{R}^3$. Let $\boldsymbol{F} := \nabla\boldsymbol{\varphi}(\boldsymbol{X}; t)$ denote the deformation gradient with the determinant $J := \det \boldsymbol{F} > 0$. The material time derivative of the deformation gradient is $\dot{\boldsymbol{F}} = \boldsymbol{l}\boldsymbol{F}$ where $\boldsymbol{l} := \nabla\boldsymbol{v}$ is the spatial velocity gradient. The boundary-value problem for a general inelastic body is governed by the balance of momentum

$$\rho_0 \ddot{\boldsymbol{\varphi}} = \operatorname{div}[\boldsymbol{\tau}/J] + \boldsymbol{\gamma} \tag{1}$$

along with prescribed displacement boundary conditions $\boldsymbol{\varphi} = \bar{\boldsymbol{\varphi}}(\boldsymbol{X}; t)$ on $\partial\mathscr{B}_t$ and traction boundary conditions $[\boldsymbol{\tau}/J]\boldsymbol{n} = \bar{\boldsymbol{t}}$ with outward normal $\boldsymbol{n}$. ρ_0 is the density and $\boldsymbol{\gamma}$ is the prescribed body force with respect to unit volume of the current con guration. Let furthermore $\boldsymbol{g} = \delta_{ab}$ denote the covariant Cartesian metric tensor or the so-called Kronecker symbol in the current con guration. Due to nearly incompressible behaviour of elastomers, we will consider the split of the elastic response into the volumetric and isochoric parts and the viscous effects are assumed to be purely isochoric

$$\bar{\boldsymbol{F}} := J^{-1/3}\boldsymbol{F}. \tag{2}$$

The unimodular part of the deformation gradient is further split into elastic and inelastic contributions

$$\bar{\boldsymbol{F}} = \boldsymbol{F}^e\boldsymbol{F}^i. \tag{3}$$

The Kirchhoff stress $\boldsymbol{\tau}$ is a function of the deformation gradient. A decoupled volumetric-isochoric structure of nite viscoelasticity is obtained by the special form of the Helmholtz free energy function for a unit reference volume

$$\Psi = U(J) + \bar{\Psi}(\boldsymbol{g}, \boldsymbol{F}^i, \boldsymbol{F}^e). \tag{4}$$

The proposed form of stored energy yields an additive decomposition of the Kirchhoff stress into spherical and deviatoric contributions

$$\begin{aligned} &\boldsymbol{\tau} = \boldsymbol{\tau}_{\text{vol}} + \boldsymbol{\tau}_{\text{iso}} \quad \text{where} \\ &\boldsymbol{\tau}_{\text{vol}} = p\boldsymbol{g}^{-1} \quad \text{and} \quad \boldsymbol{\tau}_{\text{iso}} = \mathbb{P} : \bar{\boldsymbol{\tau}} \end{aligned} \tag{5}$$

using $\bar{\boldsymbol{\tau}} := 2\partial_{\boldsymbol{g}}\bar{\Psi}(\boldsymbol{g}, \boldsymbol{F}^i, \boldsymbol{F}^e)$, $p := JU'(J)$ and the fourth-order deviatoric projection tensor $\mathbb{P}^{ab}_{cd} = [\delta^a_c\delta^b_d + \delta^a_d\delta^b_c]/2 - \delta^{ab}\delta_{cd}/3$. The isochoric part of the free energy is further decomposed into elastic and viscous contributions

$$\bar{\Psi} = \bar{\Psi}^e(\bar{\boldsymbol{C}}) + \bar{\Psi}^v(\boldsymbol{C}_e). \tag{6}$$

$\bar{\boldsymbol{C}} = \bar{\boldsymbol{F}}^T\boldsymbol{g}\bar{\boldsymbol{F}}$ and $\boldsymbol{C}_e = \boldsymbol{F}^{eT}\boldsymbol{g}\boldsymbol{F}^e$ are the unimodular part of the right Cauchy-Green tensor and the elastic right Cauchy-Green tensor[1], respectively. The above definition induces a further split of $\bar{\boldsymbol{\tau}}$ de ned in (5)$_2$

$$\begin{aligned} &\bar{\boldsymbol{\tau}} := \bar{\boldsymbol{\tau}}^e + \bar{\boldsymbol{\tau}}^v \quad \text{with} \\ &\bar{\boldsymbol{\tau}}^e := 2\partial_{\boldsymbol{g}}\bar{\Psi}^e(\bar{\boldsymbol{C}}) \ \text{ and } \ \bar{\boldsymbol{\tau}}^v := 2\partial_{\boldsymbol{g}}\bar{\Psi}^v(\boldsymbol{C}_e). \end{aligned} \tag{7}$$

2.1 Free energy function

The volumetric part of the free energy is described by the simple form

$$U(J) = \kappa(J - \ln J - 1). \tag{8}$$

κ is the bulk modulus and will be taken large enough in order to enforce the incompressibility. For the isochoric response of the material, the free energy functions $\bar{\Psi}^e$ and $\bar{\Psi}^v$ are introduced as

$$\bar{\Psi}^e(\lambda_r) := \mu N\left(\lambda_r\mathcal{L}^{-1}(\lambda_r) + \ln\frac{\mathcal{L}^{-1}(\lambda_r)}{\sinh\mathcal{L}^{-1}(\lambda_r)}\right) \tag{9}$$

and

$$\bar{\Psi}^v(\lambda^e_r) := \mu_v N_v\left(\lambda^e_r\mathcal{L}^{-1}(\lambda^e_r) + \ln\frac{\mathcal{L}^{-1}(\lambda^e_r)}{\sinh\mathcal{L}^{-1}(\lambda^e_r)}\right). \tag{10}$$

$\lambda_r = \sqrt{I_1/3N}$ and $\lambda^e_r = \sqrt{I^e_1/3N_v}$ denote the relative network stretches for the equilibrium and non-equilibrium deformations $I_1 := \operatorname{tr}\bar{\boldsymbol{C}}$ and $I^e_1 := \operatorname{tr}\boldsymbol{C}_e$ are the rst invariants of the total and elastic right Cauchy-Green tensors, respectively. μ and μ_v are the shear modulus of the elastic chain network and superimposed free chain network, whereas N and N_v are the segment numbers of the elastic and superimposed networks, respectively. The idealized model representation of a rubber network by the 8-chain model is depicted in Fig. 1.

2.2 Thermodynamical consistency

The second axiom of thermodynamics restricts the proposed model by the so-called dissipation inequality[2]

$$\mathscr{D} := \mathscr{P} - \dot{\Psi} \geq 0 \quad \text{with} \quad \mathscr{P} := \boldsymbol{S} : \frac{1}{2}\dot{\boldsymbol{C}} = \boldsymbol{\tau} : \boldsymbol{d}. \tag{11}$$

$\boldsymbol{d} := (\boldsymbol{g}\boldsymbol{l} + \boldsymbol{l}^T\boldsymbol{g})/2$ is the symmetric Eulerian rate of the deformation tensor. Following Miehe [24], the dissipation inequality can be split into spherical and unimodular parts. Since the volumetric and isochoric responses are a priori assumed to be independent, each should satisfy the inequality separately, leading to

$$\mathscr{D} = \mathscr{D}_{\text{vol}} + \mathscr{D}_{\text{iso}} \geq 0, \tag{12}$$

with

$$\begin{aligned} &\mathscr{D}_{\text{vol}} := \boldsymbol{\tau}_{\text{vol}} : \boldsymbol{d}^{\text{vol}} - \dot{U}(J) \geq 0 \quad \text{and} \\ &\mathscr{D}_{\text{iso}} := \boldsymbol{\tau}_{\text{iso}} : \boldsymbol{d}^{\text{iso}} - \dot{\bar{\Psi}} \geq 0. \end{aligned} \tag{13}$$

For the derivation of the additive split of $\boldsymbol{d} = \boldsymbol{d}^{\text{vol}} + \boldsymbol{d}^{\text{iso}}$ and the additive split of the dissipation inequality, the reader is referred to Appendix A. No volumetric viscous effects are assumed and (13)$_1$ vanishes for $p = JU'(J)$. Taking the material time derivative of the isochoric part of the free energy function (6), we obtain the following rate expression

$$\dot{\bar{\Psi}} = 2\partial_{\bar{\boldsymbol{C}}}\bar{\Psi}^e : \frac{1}{2}\dot{\bar{\boldsymbol{C}}} + 2\partial_{\boldsymbol{C}_e}\bar{\Psi}^v : \frac{1}{2}\dot{\boldsymbol{C}}_e. \tag{14}$$

[1] Although the elastic right Cauchy-Green tensor $\boldsymbol{C}_e$ is unimodular, the overline symbol $\bar{\{\cdot\}}$ is dropped from the expression in order to simplify the notation. The same applies to inelastic right Cauchy-Green tensor $\boldsymbol{C}_i$ and elastic left Cauchy-Green tensor $\boldsymbol{b}_e$.

[2] For convenience, the reference density ρ_0 appearing before $\dot{\Psi}$ is dropped from (11)$_1$ and the free energy density is de ned per unit reference volume instead of unit mass.

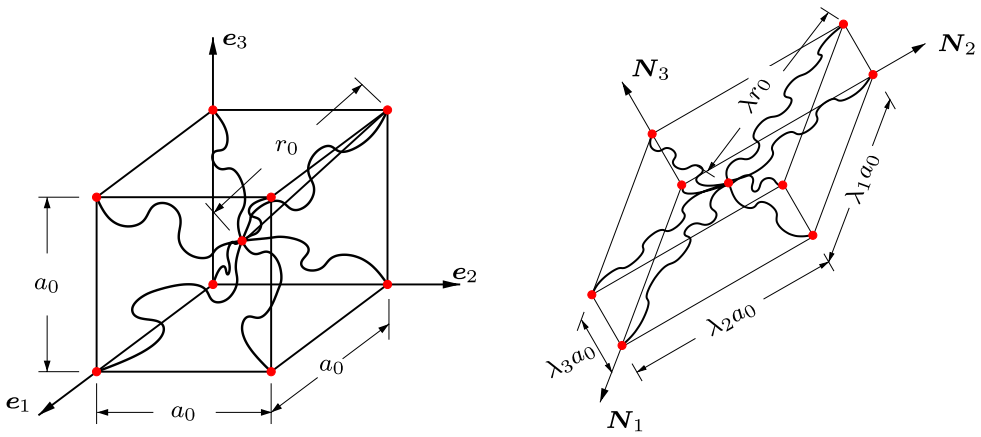

Fig. 1 8-chain model representation of rubber network in the undeformed and deformed con guration

Furthermore, the covariant rate of deformation tensor $\boldsymbol{d}^{\text{iso}} = [\boldsymbol{l}^{\text{iso}T}\boldsymbol{g} + \boldsymbol{g}\boldsymbol{l}^{\text{iso}}]/2$ in the current con guration can be de ned. Hence, $\dot{\bar{\boldsymbol{C}}}/2 = \boldsymbol{\varphi}^{*}(\boldsymbol{d}) = \bar{\boldsymbol{F}}^{T}\boldsymbol{d}^{\text{iso}}\bar{\boldsymbol{F}}$, where $\boldsymbol{\varphi}^{*}(\cdot)^{\flat} = \bar{\boldsymbol{F}}^{T}(\cdot)\bar{\boldsymbol{F}}$ is the volume preserving covariant pull-back operation. The total and elastic part of the isochoric spatial velocity gradient are related as

$$\boldsymbol{l}^{\text{iso}} = \boldsymbol{l}_e + \boldsymbol{F}^{e}\boldsymbol{l}_i\boldsymbol{F}^{e-1} = \boldsymbol{l}_e + \tilde{\boldsymbol{l}}_i. \tag{15}$$

$\tilde{\boldsymbol{l}}_i$ is the inelastic velocity gradient in the spatial con guration. This yields

$$\boldsymbol{d}^{\text{iso}} := \text{sym}(\boldsymbol{g}\boldsymbol{l}^{\text{iso}}) = \boldsymbol{d}_e + \tilde{\boldsymbol{d}}_i. \tag{16}$$

$\dot{\boldsymbol{C}}_e/2 = \boldsymbol{\varphi}^{\bar{*}}(\boldsymbol{d}_e)^{\flat} = \boldsymbol{F}^{eT}\boldsymbol{d}_e\boldsymbol{F}^{e}$ can also be de ned with $\boldsymbol{\varphi}^{\bar{*}}(\cdot)^{\flat}$ denoting the covariant pull-back operation to the intermediate con guration. Incorporating (16)$_3$ along with the expressions for $\dot{\bar{\boldsymbol{C}}}$ and $\dot{\boldsymbol{C}}_e$ into (14) leads to

$$\begin{aligned}
\dot{\bar{\Psi}} &= 2\partial_{\bar{\boldsymbol{C}}}\bar{\Psi}^{e} : [\bar{\boldsymbol{F}}^{T}\boldsymbol{d}^{\text{iso}}\bar{\boldsymbol{F}}] + 2\partial_{\boldsymbol{C}_e}\bar{\Psi}^{v} : [\boldsymbol{F}^{eT}\boldsymbol{d}_e\boldsymbol{F}^{e}] \\
&= \bar{\boldsymbol{F}}[2\partial_{\bar{\boldsymbol{C}}}\bar{\Psi}^{e}]\bar{\boldsymbol{F}}^{T} : \boldsymbol{d}^{\text{iso}} + \boldsymbol{F}^{e}[2\partial_{\boldsymbol{C}_e}\bar{\Psi}^{v}]\boldsymbol{F}^{eT} : \boldsymbol{d}_e \\
&= \bar{\boldsymbol{\tau}}^{e} : \boldsymbol{d}^{\text{iso}} + \bar{\boldsymbol{\tau}}^{v} : \boldsymbol{d}_e \qquad (17) \\
&\overset{(16)}{=} \bar{\boldsymbol{\tau}}^{e} : \boldsymbol{d}^{\text{iso}} + \bar{\boldsymbol{\tau}}^{v} : [\boldsymbol{d}^{\text{iso}} - \tilde{\boldsymbol{d}}_i] \\
&= [\bar{\boldsymbol{\tau}}^{e} + \bar{\boldsymbol{\tau}}^{v}] : \boldsymbol{d}^{\text{iso}} - \bar{\boldsymbol{\tau}}^{v} : \tilde{\boldsymbol{d}}_i.
\end{aligned}$$

Substituting (17)$_5$ into (13)$_2$ gives the dissipation inequality

$$\mathscr{D}_{\text{iso}} = \bar{\boldsymbol{\tau}}^{v} : \tilde{\boldsymbol{d}}_i \geq 0. \tag{18}$$

Since $\tilde{\boldsymbol{d}}_i$ is a deviatoric tensor, (18) can alternatively be written as

$$\mathscr{D}_{\text{iso}} = \boldsymbol{\tau}^{v}_{\text{iso}} : \tilde{\boldsymbol{d}}_i \geq 0. \tag{19}$$

2.3 Evolution law

Consistent with (19), Bergström and Boyce [1] proposed an evolution for the inelastic rate of deformation tensor in the current con guration

$$\tilde{\boldsymbol{d}}_i := \dot{\gamma}\mathbf{N}, \tag{20}$$

where

$$\mathbf{N} = \frac{\boldsymbol{\tau}^{v}_{\text{iso}}}{\|\boldsymbol{\tau}^{v}_{\text{iso}}\|} \quad \text{with} \quad \boldsymbol{\tau}^{v}_{\text{iso}} := \mathbb{P} : \bar{\boldsymbol{\tau}}^{v} \quad \text{and} \quad \|\boldsymbol{\tau}^{v}_{\text{iso}}\| := \sqrt{\boldsymbol{\tau}^{v}_{\text{iso}} : \boldsymbol{\tau}^{v}_{\text{iso}}}. \tag{21}$$

$\dot{\gamma}$ denotes the effective creep rate, and the thermodynamical consistency (19) is satis ed for $\dot{\gamma} \geq 0$. The *BB model*, constitutively describes the $\dot{\gamma}$. If a polymer network is deformed at high enough rate, both the cross-linked strong network and the superimposed entanglements deform af nely. Hence, the free dangling chains contribute to the deformation resistance. If the network is kept stretched, the dangling ends of the free chains will start moving in a combination of Brownian and reptational motion as described by Doi and Edwards [22]. A descriptive picture showing a superimposed free chain on a strong elastic network is given in Fig. 2. According to the *tube model* of Doi and Edwards [22], a function $\phi(t)$ describes the motion of a free chain

$$\phi(t) \approx \begin{cases} t^{1/2} & t \leq \tau_e \\ t^{1/4} & \tau_e \leq t \leq \tau_R \\ t^{1/2} & \tau_R \leq t \leq \tau_d \\ t & \tau_d \leq t \end{cases}, \tag{22}$$

where τ_e denotes the time at which the tube constraint is rst felt, τ_R is the Rouse relaxation time, and τ_d denotes the tube disengagement time. The effective length of the free chain can be written as

$$l(t) := l_0 + c_1\sqrt{\phi(t)}. \tag{23}$$

Bergström and Boyce [1] proposed the following expression for the inelastic network stretch

$$\lambda^{i}(t) := \frac{l(t)}{l_o} = 1 + c_2 t^{c_3}, \tag{24}$$

where, $c_2 > 0$ and $c_3 \in [0.125, 0.5]$. The time derivative of (23) yields

$$\dot{\lambda}^{i}(t) = c_2 c_3 t^{c_3 - 1}. \tag{25}$$

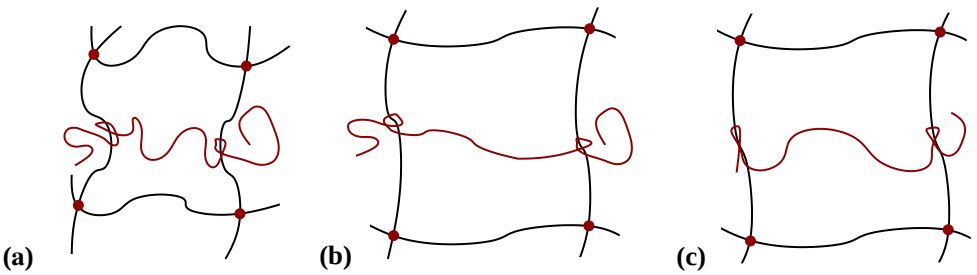

Fig. 2 Micromechanical representation of superimposed free chains in **a** undeformed, **b** deformed state after instantaneous loading and **c** deformed and relaxed state

Incorporation of $\hat{\tau}$ in (24) into (25) gives

$$\dot{\lambda}^i(t) = c_4[\lambda^i - 1]^{c_\tau}, \tag{26}$$

where $c_\tau \in [-7, -1]$. Inserting the expression (26) into (20) yields

$$\dot{\gamma} := \dot{\gamma}_0[\lambda^i_{\text{chain}} - 1]^c \left(\frac{\tau_v}{\hat{\tau}}\right)^m. \tag{27}$$

The creep process is also assumed to be energy activated. Therefore, the term $\left(\frac{\tau_v}{\hat{\tau}}\right)^m$ is added to the creep rate expression, where $\tau_v := \left\|\boldsymbol{\tau}^v_{\text{iso}}\right\|/\sqrt{2}$. $\lambda^i_{\text{chain}} := \sqrt{\frac{I^i_1}{3}}$ is the inelastic network stretch and $I^i_1 := \text{tr}\, \boldsymbol{C}_i$. $\boldsymbol{C}_i := \boldsymbol{F}^{iT}\tilde{\boldsymbol{G}}\boldsymbol{F}^i$ is the inelastic right Cauchy-Green tensor in the reference configuration, $\tilde{\boldsymbol{G}} := \delta_{\tilde{A}\tilde{B}}$ is the metric of the intermediate configuration, $\dot{\gamma}_0$ is the reference effective creep rate, $\hat{\tau}$ is a parameter introduced for dimensional purposes and has the same units as τ_v. Power term c controls the kinetics of chain relaxation, whereas m controls the energy activated inelastic flow. In order to show the effects of the material parameters c and m, a parameter study is carried out in Sect. 4.2.

The thermodynamical consistency of the *BB model* is satisfied for $\dot{\gamma}_0/\hat{\tau}^m > 0$ and $m > 0$. c is restricted by the *tube model* of Doi and Edwards [12] to be $c \in [-7, -1]$. However, to be more general, we propose $c < 0$ different from the proposition of Bergström and Boyce [1] where $c \in [-1, 0]$. By taking $c = 0$ and $m = 1$, one recovers the deviatoric part of the evolution law proposed by Reese and Govindjee [2]. Thus, we can conclude that the *BB model* is a generalized version of the finite viscoelasticity model proposed by Reese and Govindjee [2].

It should be mentioned that the micro-macro transition is achieved by linking the stretch λ^i of the single chain relaxing in a polymer chain to the term $\boldsymbol{C}_i$ of the continuum. Alternative representation of the model can be obtained by substituting $\lambda^i = \lambda/\lambda^e$ in order to avoid inelastic right Cauchy-Green tensor in the evolution law, where $\lambda^e = \sqrt{\frac{\text{tr}\, \boldsymbol{b}_e}{3}}$ and $\lambda = \sqrt{\frac{\text{tr}\, \boldsymbol{b}}{3}}$. From this substitution, it can be concluded that the *BB model* intrinsically includes dependence of the viscosity on total deformation as stated in Amin et al. [25].

3 Algorithmic setting for the constitutive model

In this section, the algorithmic setting of the model suitable for a finite element implementation will be treated. The stresses and moduli terms of the equilibrium and non-equilibrium branches will be derived. Furthermore, we propose an efficient implicit update for the principle elastic stretches of the viscous branch, conceptually following the work of Reese and Govindjee [2].

3.1 Stress and moduli terms for the elastic part

The Kirchhoff stresses and the Eulerian moduli terms corresponding to the volumetric part of the deformation can be defined as

$$\boldsymbol{\tau}_{\text{vol}} := 2\partial_{\boldsymbol{g}} U(J) \quad \text{and} \quad \mathbb{C}_{\text{vol}} := 4\partial^2_{\boldsymbol{g}\boldsymbol{g}} U(J). \tag{28}$$

Taking the necessary derivatives, we end up with

$$\boldsymbol{\tau}_{\text{vol}} = p\boldsymbol{g}^{-1} \quad \text{and} \quad \mathbb{C}_{\text{vol}} = (p+s)\boldsymbol{g}^{-1}\otimes\boldsymbol{g}^{-1} - 2p\mathbb{I}, \tag{29}$$

where $\mathbb{I}^{abcd}_{\boldsymbol{g}^{-1}} := [\delta^{ac}\delta^{bd} + \delta^{ad}\delta^{bc}]/2$ is the fourth order identity tensor.

$$p := JU'(J) \quad \text{and} \quad s := J^2U''(J) \tag{30}$$

are the hydrostatic Kirchhoff stresses (negative pressure) and corresponding modulus, respectively. The deviatoric stresses and moduli read

$$\begin{aligned}\boldsymbol{\tau}_{\text{iso}} &= \mathbb{P} : \bar{\boldsymbol{\tau}} \quad \text{and} \\ \mathbb{C}_{\text{iso}} &= \mathbb{P} : [\bar{\mathbb{C}} + \tfrac{2}{3}(\bar{\boldsymbol{\tau}} : \boldsymbol{g})\mathbb{I} - \tfrac{2}{3}(\bar{\boldsymbol{\tau}}\otimes\boldsymbol{g}^{-1} + \boldsymbol{g}^{-1}\otimes\bar{\boldsymbol{\tau}})] : \mathbb{P}\end{aligned} \tag{31}$$

where

$$\bar{\mathbb{C}} := \bar{\mathbb{C}}^e + \bar{\mathbb{C}}^v_{\text{algo}}. \tag{32}$$

$\bar{\mathbb{C}}^e := 4\partial^2_{\boldsymbol{g}\boldsymbol{g}}\bar{\Psi}^e(\lambda_r)$ denote the elasticity moduli of the equilibrium response. The algorithmic consistent moduli $\bar{\mathbb{C}}^v_{\text{algo}}$ for the non-equilibrium response will be explained in the next section. The stress and moduli expressions of the equilibrium response are derived from (9) as

$$\bar{\boldsymbol{\tau}}^e = \frac{\mu}{3}\frac{\mathcal{L}^{-1}(\lambda_r)}{\lambda_r}\bar{\boldsymbol{b}} \quad \text{and} \quad \bar{\mathbb{C}}^e = \frac{4}{9}\frac{\mu}{N}\frac{1}{(1-\lambda_r^2)^2}\bar{\boldsymbol{b}}\otimes\bar{\boldsymbol{b}}. \tag{33}$$

$\bar{\boldsymbol{b}} = \bar{\boldsymbol{F}}\boldsymbol{G}^{-1}\bar{\boldsymbol{F}}^T$ is the unimodular part of the Finger tensor, and $\boldsymbol{G}$, where $G_{AB} := \delta_{AB}$, is the reference metric. In the above equation, the inverse Langevin function is computed by Padé approximation $\mathcal{L}^{-1}(\lambda_r) \approx \lambda_r(3-\lambda_r^2)/(1-\lambda_r^2)$ proposed by Cohen [25]. It is superior to the polynomial approximations with a simple form. It shows the singular behaviour of the inverse Langevin function at $\lambda_r = 1$ and exhibits very good results. Diani and Gilormini [27] have reported that the error associated with the Padé approximation does not exceed 5%, where the approximation is reported to yield exact results at $\lambda_r = 0$ and around the limit $\lambda_r = 1$ and the deviation steadily increases from $\lambda_r = 0$ attaining a maximum of relative error $\approx 5\%$ around $\lambda_r = 0.8$.

3.2 Stress and moduli terms for the viscous part

From $(7)_3$, the viscous part of the Kirchhoff stresses can be evaluated as

$$\bar{\boldsymbol{\tau}}^v = \frac{\mu_v}{3}\frac{\mathcal{L}^{-1}(\lambda_r^e)}{\lambda_r^e}\boldsymbol{b}_e. \tag{34}$$

In order to compute the expression (34), one needs the current value of $\boldsymbol{b}_e$ at time $t = t_{n+1}$. The computation of $\boldsymbol{b}_e$ depends on the treatment of evolution law which will be explained in the next subsection.

3.2.1 Integration of the evolution law

The kernel of the subsequent treatment depends on the identity

$$-\frac{1}{2}\pounds_v\boldsymbol{b}_e \cdot \boldsymbol{b}_e^{-1} = \tilde{\boldsymbol{d}}_i. \tag{35}$$

The integration of the evolution law is based on an operator split of the material time derivative of $\boldsymbol{b}_e$ into an elastic predictor (E) and an inelastic corrector step (I) as

$$\dot{\boldsymbol{b}}_e := \underbrace{\boldsymbol{l}^{\text{iso}}\boldsymbol{b}_e + \boldsymbol{b}_e\boldsymbol{l}^{\text{iso}T}}_{E} + \underbrace{\pounds_v\boldsymbol{b}_e}_{I}. \tag{36}$$

$\pounds_v\boldsymbol{b}_e := \bar{\boldsymbol{F}}\dot{\overline{\boldsymbol{C}_i^{-1}}}\bar{\boldsymbol{F}}^T$ is a unimodular operator similar to the Lie time derivative of the elastic Finger tensor.

During the *elastic trial step*, $\dot{\overline{\boldsymbol{C}_i^{-1}}}$ is equal to zero. Therefore,

$$(\boldsymbol{C}_i^{-1})_{tr} = (\boldsymbol{C}_i^{-1})_{t_n} \rightarrow \boldsymbol{b}_e{}^{tr} = \bar{\boldsymbol{F}}(\boldsymbol{C}_i^{-1})_{t_n}\bar{\boldsymbol{F}}^T. \tag{37}$$

The subscript denoting the current time step t_{n+1} is dropped for convenience. The asset of this proposal is to circumvent the rate of inelastic metric in computation of the consistent tangent moduli.

In the inelastic corrector step, $\boldsymbol{l} = \boldsymbol{l}^{\text{iso}} + \boldsymbol{l}^{\text{vol}}$ is set to zero leading $\pounds_v\boldsymbol{b}_e = \dot{\boldsymbol{b}}_e$. Consequently, we have the following for the evolution law

$$\dot{\boldsymbol{b}}_e = [-2\dot{\gamma}\mathbf{N}]\boldsymbol{b}_e{}^{tr}. \tag{38}$$

The equation can be solved by the so-called exponential mapping. This yields the expression

$$\boldsymbol{b}_e = \exp\left[-2\int_{t_n}^{t_{n+1}}\dot{\gamma}\mathbf{N}dt\right]\boldsymbol{b}_e{}^{tr}. \tag{39}$$

Approximating the integral equation, we obtain

$$\boldsymbol{b}_e \approx \exp\left[-2\dot{\gamma}\mathbf{N}\Delta t\right]\boldsymbol{b}_e{}^{tr}. \tag{40}$$

Due to isotropy, $\boldsymbol{\tau}^v_{\text{iso}}$ and consequently $\mathbf{N}$ commute with $\boldsymbol{b}_e$ and also with $\boldsymbol{b}_e{}^{tr}$. Hence, (39) can be written in the principal stretch directions

$$\lambda_a^{e2} \approx \exp\left[-\frac{2}{\|\text{dev}\tau^v\|}\Delta t\dot{\gamma}\,\text{dev}\tau_a\right]\lambda_a^{etr2}. \tag{41}$$

Introducing elastic principal logarithmic stretches $\varepsilon_a = \ln\lambda_a^{etr}$, and taking the logarithm of (41), we obtain

$$\varepsilon_a \approx -\frac{\Delta t}{\sqrt{2}}\frac{\dot{\gamma}}{\tau_v}\,\text{dev}\tau_a + \varepsilon_a^{tr}. \tag{42}$$

(42) constitutes a nonlinear relation since τ_a and $\dot{\gamma}$ are also a function of principal stretches. Hence, the residual expression for iterative solution will be de ned

$$r_a := \varepsilon_a + \frac{\Delta t}{\sqrt{2}}\frac{\dot{\gamma}}{\tau_v}\,\text{dev}\tau_a - \varepsilon_a^{tr} = 0. \tag{43}$$

The steps of the local Newton iteration are summarized in Table 1. The derivation of the local tangent $\mathcal{K}$ is shown in Appendix B. During the computation of the residual tangent $\mathcal{K}$, inelastic network stretch is frozen such that $\lambda^i_{\text{chain}} = \lambda^i_{\text{chain}}|_{t_n}$ in order to avoid the partial derivative $\frac{\partial\lambda^i_{\text{chain}}}{\partial\varepsilon_b}$. This is due to the fact that the $\boldsymbol{e}^i$ and $\boldsymbol{b}_e$ do not lie in the same eigenspace. This assumption disturbs the unconditional stability of the implicit update scheme used. However, as shown is Sect. 4.5, the algorithm is robust with no indication stability problems. The computational time is improved significantly, since lengthy tensorial operations are avoided in the internal iteration step.

3.2.2 Algorithmic moduli for the viscous part

In this section, we will set up a closed-form expression for the so-called consistent tangent moduli for the viscous part. The spectral decomposition of the trial elastic deformation yields

$$\boldsymbol{F}_e^{tr} = \sum_{a=1}^{3}\lambda_a^{etr}\,\boldsymbol{n}_a \otimes \boldsymbol{N}^a. \tag{44}$$

Table 1 Steps of local Newton iteration

1. Set initial values	$k = 0, \varepsilon_a^k = \varepsilon_a^{tr}$
DO	
2. Residual equation	$r_a := \varepsilon_a + \frac{\Delta t}{\sqrt{2}} \frac{\dot{\gamma}}{\tau_v} \text{dev} \tau_a - \varepsilon_a^{tr} = 0$
3. Linearization	$\text{Lin} r_a = r_a\|_{\varepsilon^k} + \left. \frac{\partial r_a}{\partial \varepsilon_b} \right\|_{\varepsilon = \varepsilon^k} \Delta \varepsilon_b^k = 0$
4. Compute	$\mathcal{K}_{ab} := \left. \frac{\partial r_a}{\partial \varepsilon_b} \right\|_{\varepsilon = \varepsilon^k}$
5. Solve	$\Delta \varepsilon_a^k = -\mathcal{K}_{ab}^{-1} r_a$
6. Update	$\varepsilon_a^{k+1} \leftarrow \varepsilon_a^k + \Delta \varepsilon_a^k$
	$k \leftarrow k + 1$
WHILE	$TOL \leq \|r_a\|$

We de ne the ctitious second Piola-Kirchhoff stress tensor

$$\tilde{\boldsymbol{S}}^v := \boldsymbol{F}_e^{tr\,-1} \bar{\boldsymbol{\tau}}^v \boldsymbol{F}_e^{tr\,-T}; \quad \tilde{\boldsymbol{S}}^v = \sum_{a=1}^{3} \frac{\tau_a}{\lambda_a^{e\,tr\,2}} \boldsymbol{N}_a \otimes \boldsymbol{N}_a \tag{45}$$

in the intermediate con guration. With the definition (45)$_1$ at hand, the incremental rate equation can be de ned

$$\Delta \tilde{\boldsymbol{S}} = \bar{\mathbb{C}}_{\text{algo}}^v : \Delta \boldsymbol{C}_e^{\,tr} \tag{46}$$

where

$$\bar{\mathbb{C}}_{\text{algo}}^v = 2 \partial_{\boldsymbol{C}_e^{tr}} \tilde{\boldsymbol{S}}. \tag{47}$$

Exploiting (47), starting from (45)$_2$, we end up with the moduli expression

$$\bar{\mathbb{C}}_{\text{algo}}^v = \sum_{a=1}^{3} \sum_{b=1}^{3} \frac{c_{ab} - 2\tau_a \delta_{ab}}{\lambda_a^{e\,tr\,2} \lambda_a^{e\,tr\,2}} \boldsymbol{N}_a \otimes \boldsymbol{N}_a \otimes \partial_{\boldsymbol{C}_e^{tr}} \lambda_b^{e\,tr\,2} + \sum_{a=1}^{3} \frac{2\tau_a}{\lambda_a^{e\,tr\,2}} \partial_{\boldsymbol{C}_e^{tr}} (\boldsymbol{N}_a \otimes \boldsymbol{N}_a). \tag{48}$$

The partial derivatives are given by

$$\partial_{\boldsymbol{C}_e^{tr}} \lambda_b^{e\,tr\,2} = \boldsymbol{N}_b \otimes \boldsymbol{N}_b \tag{49}$$

and

$$\partial_{\boldsymbol{C}_e^{tr}} (\boldsymbol{N}_a \otimes \boldsymbol{N}_a) = \sum_{b \neq a}^{3} \frac{1}{2} \frac{1}{\lambda_a^{e\,tr\,2} - \lambda_b^{e\,tr\,2}} (\mathbb{G}_{ab} + \mathbb{G}_{ba}) \tag{50}$$

where $\mathbb{G}_{ab}^{IJKL} := M_a^{IK} M_b^{JL} + M_a^{IL} + M_b^{JK}$ with

$$\boldsymbol{M}_a := \boldsymbol{N}_a \otimes \boldsymbol{N}_a \quad \text{and} \quad M_a^{IJ} := N_a^I N_a^J. \tag{51}$$

After incorporation of (49) and (50) into (48), we nally obtain the compact definition of the moduli expression

$$\bar{\mathbb{C}}_{\text{algo}}^v = \sum_{a=1}^{3} \sum_{b=1}^{3} \frac{c_{ab} - 2\tau_a \delta_{ab}}{\lambda_a^{e\,tr\,2} \lambda_b^{e\,tr\,2}} \boldsymbol{M}_a \otimes \boldsymbol{M}_b + \sum_{a \neq b}^{3} \sum_{b=1}^{3} \frac{1}{2} \frac{\tilde{s}_a - \tilde{s}_b}{\lambda_a^{e\,tr\,2} - \lambda_b^{e\,tr\,2}} (\mathbb{G}_{ab} + \mathbb{G}_{ba}), \tag{52}$$

with $\tilde{s}_a = \tau_a / \lambda_a^{e\,tr\,2}$. In (52), the term c_{ab} is de ned as

$$c_{ab} := \frac{\partial \tau_a}{\partial \varepsilon_b^{tr}} = \frac{\partial \tau_a}{\partial \varepsilon_c} \frac{\partial \varepsilon_c}{\partial \varepsilon_b^{tr}}, \tag{53}$$

and for the derivation, we recall the residual expression of the local Newton iteration. The total derivative of the residual expression with respect to trial stretches yields

$$\frac{dr_a}{d\varepsilon_b^{tr}} = \frac{\partial r_a}{\partial \varepsilon_b^{tr}} + \frac{\partial r_a}{\partial \varepsilon_c} \frac{\partial \varepsilon_c}{\partial \varepsilon_b^{tr}} = 0 = -\delta_{ab} + \mathcal{K}_{ac} \frac{\partial \varepsilon_c}{\partial \varepsilon_b^{tr}} = 0. \tag{54}$$

Hence, we obtain the expression

$$\frac{\partial \varepsilon_a}{\partial \varepsilon_b^{tr}} = \mathcal{K}_{ab}^{-1}. \tag{55}$$

Inserting (55) and (B.9) into (53), we nally end up with

$$c_{ab} = \mathcal{T}_{ac}\, \mathcal{K}_{cb}^{-1}. \tag{56}$$

However, expression (52) is still in the ctitious intermediate con guration. By executing the push-forward operation via $\boldsymbol{F}_e^{tr}$, the algorithmic moduli expression in the current con guration

$$\bar{\mathbb{C}}_{\text{algo}}^{v\;ijkl} = F_e^{tr\,i}{}_I\, F_e^{tr\,j}{}_J\, F_e^{tr\,k}{}_K\, F_e^{tr\,l}{}_L\, \bar{\mathbb{C}}_{\text{algo}}^{v\;IJKL} \tag{57}$$

is obtained.

The moduli expression (52) has a singularity for equal eigenvalues $\lambda_a^{e\,tr} = \lambda_b^{e\,tr}$

$$\lim_{\lambda_a^{e\,tr} \to \lambda_b^{e\,tr}} \frac{\tilde{s}_a - \tilde{s}_b}{\lambda_a^{e\,tr\,2} - \lambda_b^{e\,tr\,2}} = \frac{0}{0}. \tag{58}$$

Recalling L'Hospital's rule

$$\lim_{x \to a} \frac{f(x)}{g(x)} = \lim_{x \to a} \frac{f'(x)}{g'(x)} \quad \text{if} \quad \lim_{x \to a} \frac{f(x)}{g(x)} = \frac{0}{0} \tag{59}$$

and applying (59) to (58) we obtain

$$\lim_{\lambda_a^{e\,tr} \to \lambda_b^{e\,tr}} \frac{\tilde{s}_a - \tilde{s}_b}{\lambda_a^{e\,tr\,2} - \lambda_b^{e\,tr\,2}} = \frac{1}{2} \frac{c_{aa} - 2\tau_a}{\lambda_a^{e\,tr\,4}}. \tag{60}$$

The rest of the division by zero problems, e.g. (21), can be overcome by the perturbation of the denominator.

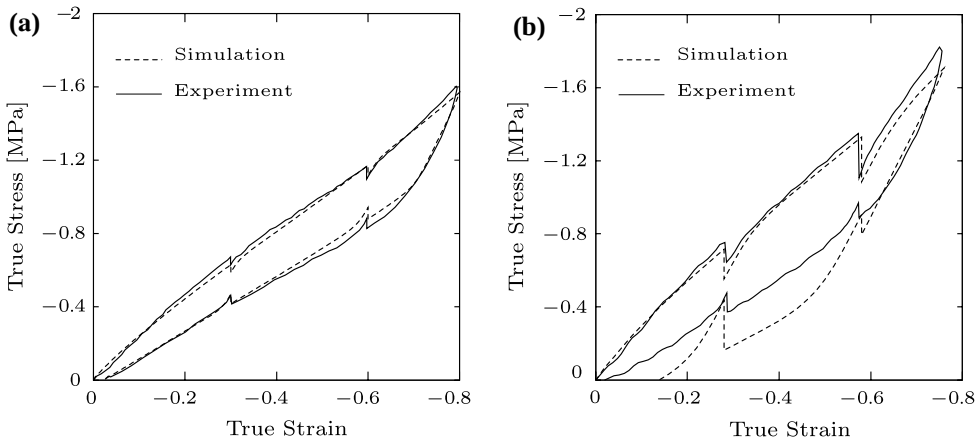

Fig. 3 Compression test with intermittent relaxation. **a** True strain rate $\dot{\varepsilon} = -0.002\ s^{-1}$, **b** true strain rate $\dot{\varepsilon} = -0.01\ s^{-1}$. Experiments are taken from Bergström and Boyce [1]

4 Numerical examples

In this section, we will assess the capability of the proposed algorithmic setting and the material model. Firstly, we will validate the proposed implementation with a given uniaxial compression test. Then, a parameter study will be performed in order to give a deeper understanding to the appearing parameters in the evolution law. The fitting capability of the constitutive model with respect to recent experimental data on rubber viscoelasticity will be considered. A representative boundary value problem will be investigated in order to show the capability of the proposed algorithmic setting. Finally, the convergence and the stability of the proposed algorithmic setting will be discussed. For this purpose, the formulation described in the previous section is implemented into the general-purpose finite element program FEAP originally developed by R.L. Taylor. For the boundary value problem, the mixed Jacobian-pressure formulation (Q1/P0 element) proposed by Simo et al. [28] is used. A more compact representation of Q1/P0 element is documented in Miehe [29]. For this type of formulations, the volumetric stresses (28) and moduli terms (29) drop from the formulation and the incompressibility is enforced on the element level. The bulk modulus κ taken in the subsequent sections acts as a penalty parameter at element level.

4.1 Example 1

In the first numerical example, we consider the uniaxial compression test with intermittent relaxation time as a benchmark problem. The material is subjected to true strain rates of $\dot{\varepsilon} = -0.002\ s^{-1}$ and $\dot{\varepsilon} = -0.1\ s^{-1}$ with 120 s relaxation time at $\varepsilon = -0.3$ and $\varepsilon = -0.6$, respectively. The experimental results are taken from Bergström and Boyce [1]. The material parameters used are taken identically to the ones proposed by the authors and are $\kappa = 1{,}000$ MPa, $\mu = 0.6$ MPa, $\mu_v = 0.96$ MPa, $N = 8$, $N_v = 8$, $\dot{\gamma}_0/\hat{\tau}^m = 7\ s^{-1}\text{MPa}^{-m}$, $c = -1$ and $m = 4$. The proposed algorithmic implementation yields results identical to the ones proposed by Bergström and Boyce [1] (see Fig. 3). This justifies the assumptions made for the proposed algorithm. It should however be kept in mind that the evolution law is singular at the beginning of the loading process where $\lambda^i_{\text{chain}} = 1$. In order to overcome this problem, a perturbation parameter ϵ is added to the term $[\lambda^i_{\text{chain}} - 1 + \epsilon]^c$ by Bergström and Boyce [30]. Due to the power term $c < 0$, the perturbation parameter ϵ should be adjusted in order to overcome the singularity at the first few steps of the loading process. After validation of the proposed algorithm, we investigate the sensitivity of the model with respect to the material parameters in the evolution law. The uniaxial compression test described is used for the investigation with $\dot{\varepsilon} = -0.002$. The sensitivity of the model with respect to parameters $\dot{\gamma}_0/\hat{\tau}^m$ and m is depicted in Fig. 4. In Fig. 4a, all the other parameters are taken as given above. The smaller the value of $\dot{\gamma}_0/\hat{\tau}^m$, the more significant is the hysteresis. On the other hand, as seen in Fig. 4b, the greater the value of m, the greater is the hysteresis. In Fig. 5a and Fig. 5b, the effect of the parameter c in the range of $c \in [-1, 0]$ and $c \leq -1$ is studied, respectively. As the value of $|c|$ increases, the amount of hysteresis decreases. However, the slope is steeper at the beginning of the loading process, then the curve attains a certain offset.

4.2 Example 2

In the second example, we carry out a parametric investigation of the evolution law. The material parameters are taken as $\kappa = 1{,}000$ MPa, $\mu = 0.6$ MPa, $\mu_v = 0.96$ MPa, $N = N_v = 8$ and $\dot{\gamma}_0/\hat{\tau}^m = 0.07\ s^{-1}\text{MPa}^{-m}$. Taking the parameter $c = 0$ and $m = 1$, the model recovers the isochoric part of the evolution law proposed by Reese and Govindjee [2]. In Fig. 6a, normalized relaxation curves for stretch levels $\lambda = 1.1$, $\lambda = 1.5$ and $\lambda = 2.0$ are plotted against time. For $\lambda = 1.1$, the deviation is small from thermodynamical equilibrium and the relaxation curve approaches to the so-called finite linear

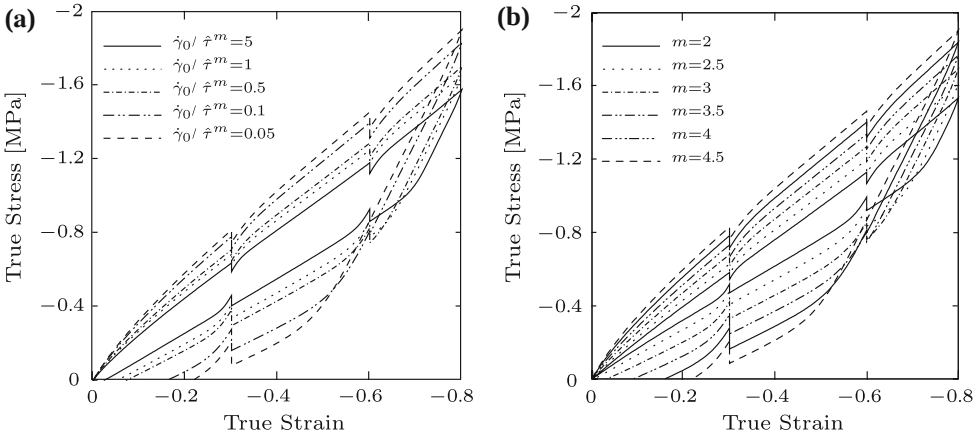

Fig. 4 Sensitivity of the model with respect to material parameter $\dot{\gamma}_0/\hat{\tau}^m$ and m: **a** $\dot{\gamma}_0/\hat{\tau}^m$ = [0.05, 0.1, 0.5, 1.0, 5], **b** m = [2, 2.5, 3.0, 3.5, 4.0, 4.5]

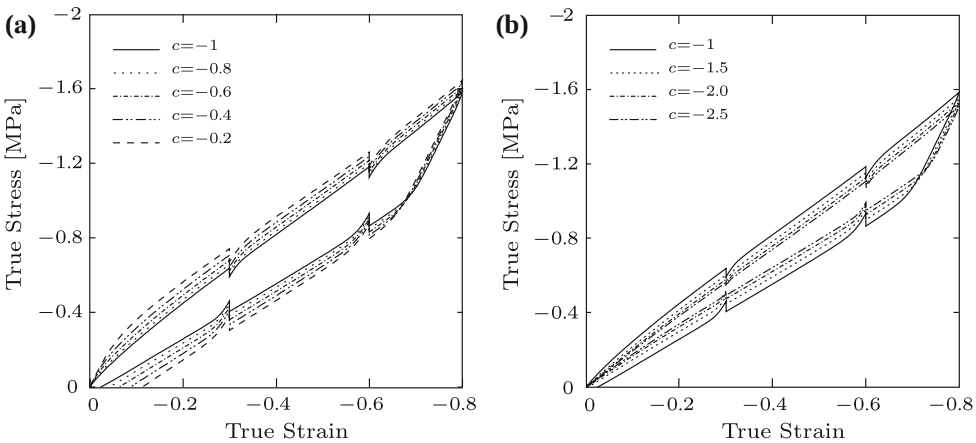

Fig. 5 Sensitivity of the model with respect to material parameter c: **a** c = [−1, −0.8, −0.6, −0.4, −0.2], **b** c = [−1, −1.5, −2, −2.5]

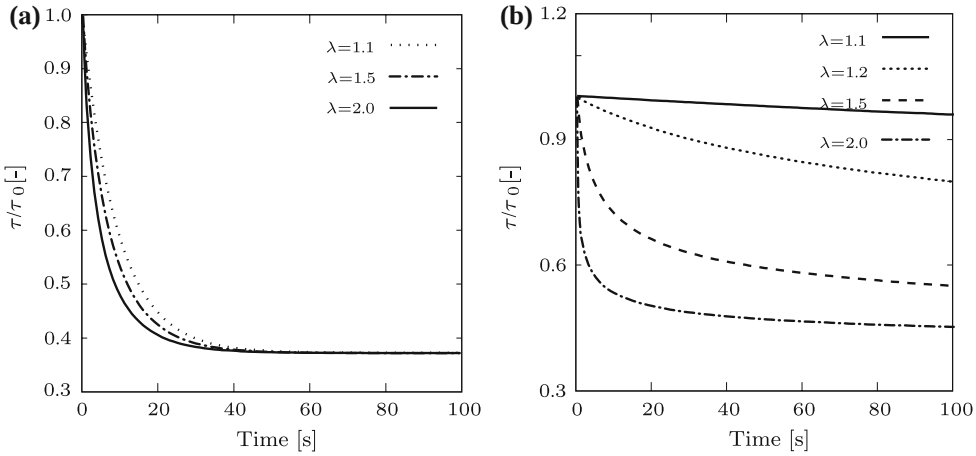

Fig. 6 Normalized relaxation curves: **a** Parameters $s = 0$ and $m = 1$ yield a materially linear evolution law. **b** The evolution law is purely energy activated for parameters $s = 0$ and $m = 4$

viscoelasticity models. The higher the stretch level, the steeper the descent of the curves as a consequence of geometrically induced nonlinearity in the evolution law. Figure 6b shows the relaxation curves solely due to an energy activated evolution law ($c = 0$ and $m = 4$). In this case, the viscous dashpot is not activated until a certain energy barrier is overcome. This enables us to model amplitude dependent hysteresis. Figure 7a deals with the part of the evolution law with respect to relaxation kinetics of a dangling chain in a fixed elastic network, inspired by Doi and Edwards [32]. It is noteworthy to mention that the steep initial slope is associated with the singularity of the evolution law at $\lambda_{\text{chain}}^{i} = 1$. Figure 7b depicts the stress relaxation curves of the *model* for $m = 4$ and $c = -1$ at different stretch levels.

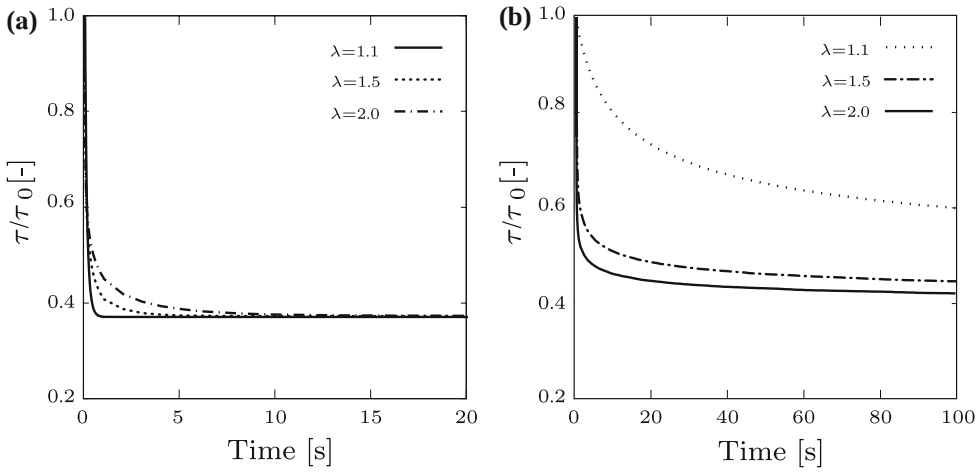

Fig. 7 Normalized relaxation curves: **a** Parameters $s = -1$ and $m = 1$ depict relaxation kinetics of entanglements. **b** The *BB model* with arbitrary parameters $m = 4$ and $c = -1$

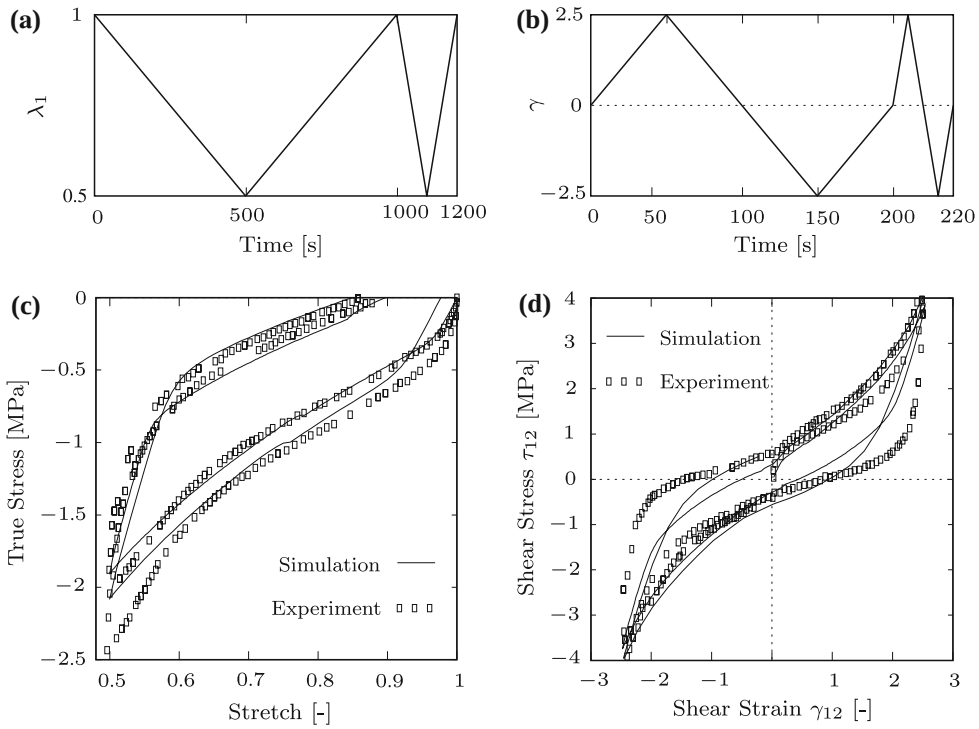

Fig. 8 Numerical simulation of cyclic **c** uniaxial compression, **d** simple shear tests of HDR at different strain rates. Experiments are taken from Amin et al. [25]. **a** and **b** shows the corresponding loading curves to **c** and **d**, respectively

4.3 Example 3

In this example, the modeling capabilities of the *BB model* will be investigated with respect to recently published experimental data. Amin et al. [25] proposed a new evolution law based on the finite viscoelasticity constitutive framework of Huber and Tsakmakis [31]. They have reported different rate sensitivities for loading and unloading for high damping rubbers (HDR) and natural rubber (NR) under simple shear and uniaxial compression loading. Taking different rate sensitivities associated with loading and unloading into account, they proposed a nonlinear viscosity law $\dot{\gamma} = f(\boldsymbol{\tau} : \boldsymbol{d}, \boldsymbol{b}, \mathrm{dev}\bar{\boldsymbol{\tau}}^v)$ as a function of total deformation, non-equilibrium stress and stress power. The sign of the stress power is utilized in order to attach different viscosities to loading and unloading processes. The Figures 30 and 31 of Amin et al. [25] are taken as a benchmark for comparison with the *BB model*. Loading rates are depicted in Fig. 8a and b. The experimental results for uniaxial compression and simple shear are depicted in Fig. 8c and d. The same material parameters are used for both compression and shear tests. The identified parameters are $\kappa = 500\,\mathrm{MPa}$, $\mu = 0.70\,\mathrm{MPa}$, $\mu_v = 2.0\,\mathrm{MPa}$, $N = 5.5$, $N_v = 6$, $\dot{\gamma}_0/\hat{\tau}^m = 0.2\,\mathrm{s}^{-1}\,\mathrm{MPa}^{-m}$, $c = -0.8$ and $m = 4$. The perturbation parameter $\epsilon = 0.02$ is used in order to regularize the singularity around $\lambda_{\mathrm{chain}}^i \approx 1$. Under uniaxial compression, the agreement of the *BB model* with the experiment is quite good (see Fig. 8c). For simple shear tests, loading curves are in better correlation than unloading curves.

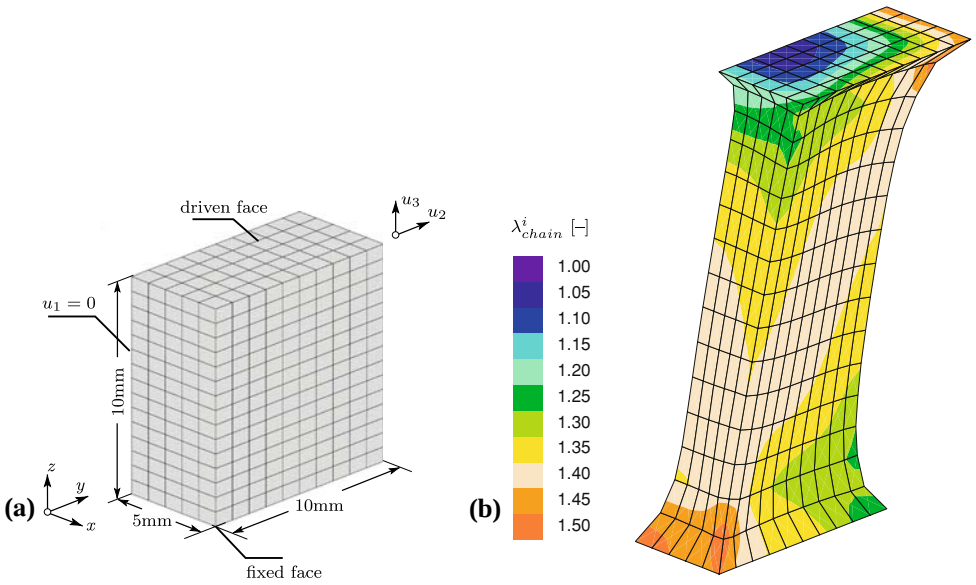

Fig. 9 Finite element analysis of a cube driven in lateral and longitudinal directions: **a** Geometry, boundary conditions and FE discretization, **b** deformed shape at $t = 10\,\mathrm{s}$, contour plots depict the inelastic network stretch λ^i_{chain}

The parameter sets improve for both compression and shear tests if the identification process takes into account a single mode of loading. In both uniaxial compression and simple shear tests, the *BB model* is in a better agreement with the experimental data than the model proposed by Amin et al. [25].

4.4 Example 4

In the following, we investigate the model response for a three-dimensional boundary value problem. During numerical simulation, different strain rates as well as nonhomogeneous deformation states are involved at each material point. Hence, it allows us to evaluate the overall response of the algorithmic setting proposed. The geometry and the boundary conditions of the problem are depicted in Fig. 9a. All degrees of freedom are fixed at the bottom surface. At top surface, the specimen is driven with $u_2 = u_3 = u(t)$, whereas displacement in x-direction is held constant, $u_1 = 0$. Due to symmetry, only half of the cube is discretized leading to $u_1 = 0$ at $x = 0$. The FE-mesh consists of $5 \times 10 \times 15$ Q1/P0 brick elements. The specimen is monotonically loaded with a tip displacement rate $\dot{u}(t) = 10\,\mathrm{mm/s}$ up to $t = 1\,\mathrm{s}$ and kept stretched for relaxation. The incremental loading is performed at constant time step $\Delta t = 0.04\,\mathrm{s}$. The deformed configuration and the distribution of inelastic network stretch at $t = 10\,\mathrm{s}$ is depicted in Fig. 9b. The material parameters used are identical to those of the first example. The FE-analysis shows that the numerical implementation is very efficient and quadratic convergence is observed which validates the performance of the proposed algorithmic setting.

4.5 Convergence and stability

As mentioned before, an explicit update of the λ^i_{chain} destroys the unconditional stability of the backward Euler scheme adopted for the integration of the evolution law. The effect of this assumption on the global stability and convergence behaviour of the boundary value problem is investigated using the material parameters given in Sect. 4.3. A square cuboid with dimensions $25 \times 25 \times 20\,\mathrm{mm}$ (height $= 20\,\mathrm{mm}$) is subjected to uniaxial tension and macroscopic simple shear. Half of the cuboid is analysed due to symmetry. The FE-mesh consists of $10 \times 5 \times 10$ Q1/P0 brick elements. In the first set of experiments, the cuboid is subjected to a uniaxial tension up to $\lambda = 3.5$ with a loading rate of $\dot{\lambda} = 0.05/\mathrm{s}$. The specimen is investigated for time increments $\Delta t = 0.5\,\mathrm{s}, \Delta t = 1.0\,\mathrm{s}$, $\Delta t = 2.0\,\mathrm{s}, \Delta t = 4.0\,\mathrm{s}$, respectively. Stress-stretch curves for different time increments are depicted in Fig. 10. The simulations are repeated for $c = 0$ and $c = -0.8$. For $c = 0$, the material law does not include the chain relaxation kinetics and the algorithm proposed is implicitly updated totally. For $c = 0$, the simulation begins with an initial shear modulus $\mu + \mu_v$ (Fig. 10a) whereas for $c = -0.8$, due to initially zero viscosity, the shear modulus is equivalent to the shear modulus of the elastic branch (see Fig. 10b). The accuracy of the of the algorithm is satisfactory even at large time increments. The number of iterations per time step is shown in Fig. 12a. The interesting outcome of the investigation is that there is no sign of deterioration in the convergence for $c = -0.8$. The above mentioned procedure is repeated for simple shear up to macroscopic shear strain $\gamma = 2.5$ and $\dot{\gamma} = 0.05/\mathrm{s}$ (see Fig. 11). The simulation reveals non-homogeneous deformations satisfying the macroscopic simple shear deformation in

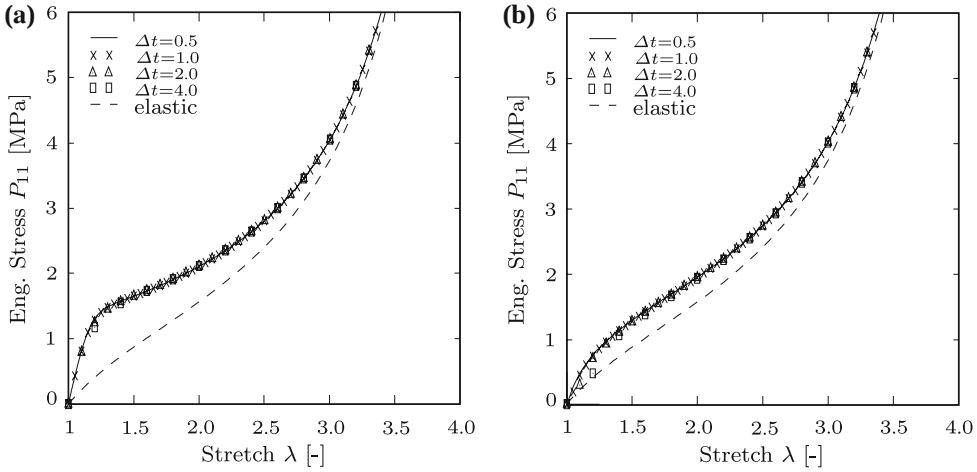

Fig. 10 Engineering stress versus stretch curves for **a** $c = 0$ and **b** $c = -0.8$, respectively. Solution for incremental time steps $\Delta t = 0.5\,\mathrm{s}, \Delta t = 1\,\mathrm{s}$, $\Delta t = 2\,\mathrm{s}, \Delta t = 4\,\mathrm{s}$ and a reference elastic solution $\Delta t = 0.5\,\mathrm{s}$ are given

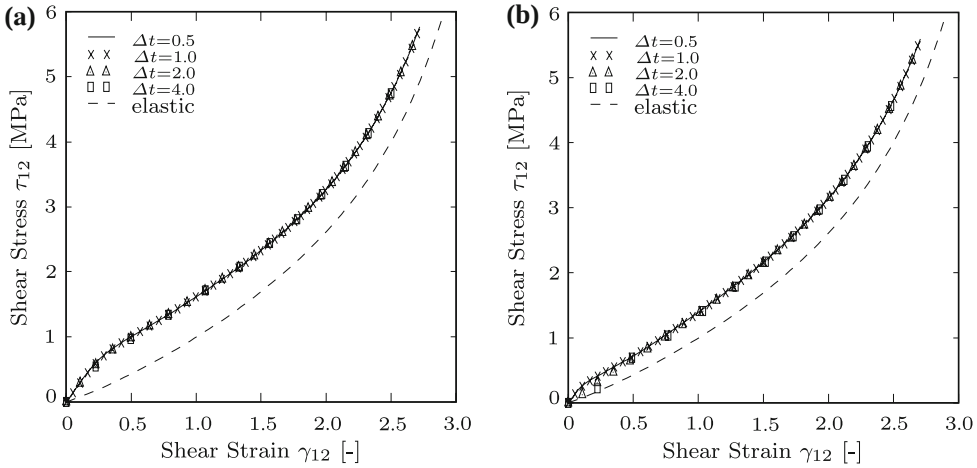

Fig. 11 Shear stress versus strain curves for **a** $c = 0$ and **b** $c = -0.8$, respectively. Solution for incremental time steps $\Delta t = 0.5\,\mathrm{s}, \Delta t = 1\,\mathrm{s}$, $\Delta t = 2\,\mathrm{s}, \Delta t = 4\,\mathrm{s}$ and a reference elastic solution $\Delta t = 0.5\,\mathrm{s}$ are given

an average-sense as expected. Stress-stretch curves for different time increments are depicted in Fig. 10. For $c = -0.8$, the number of iterations per time increments are depicted in Fig. 12b. Except for the first few iterations where the model includes a singularity at $\lambda^i_{\text{chain}} = 1$, the convergence is quadratic (Fig. 12c). The problem can be overcome by increasing parameter ϵ ($\epsilon = 0.001$ is taken throughout the simulations). This is related to the physics of the problem where the relaxation time approaches zero (see Fig. 7a). For accuracy, small time steps should be preferred at the beginning where $\lambda^i_{\text{chain}} \approx 1$.

Uniaxial tension simulations show quadratic convergence independent of the time increment. Under simple shear, the global FE solution is quadratically convergent for the reference elastic solution for both small and large time increments. The number of iterations is higher at the first few time steps for larger time increments. Viscoelastic simulations show better convergence compared to the reference elastic solution. For the case $c \neq 0$, the number of iterations is higher at the beginning. At later stages, the convergence behaviour is identical for the cases $c = 0$ and $c \neq 0$. Higher number of iterations (only one iteration in this special case) for $c \neq 0$ is related to the singularity at the beginning. The algorithm is very stable and does not terminate as long as the reference elastic solution is convergent. Introduced viscosity improves the convergence of the elastic reference solution.

5 Conclusion

We proposed an algorithmic setting for Bergström–Boyce finite viscoelasticity model suitable for the finite element method. We revisited the thermodynamical requirements and proved the consistency of the model based on the dissipation inequality. Since the viscous deformations occur solely in the isochoric plane, the dissipation inequality is split into isochoric and volumetric contributions consistent to the additive split of the free energy function. Hence, the thermodynamical consistency of the evolution law is proved for the isochoric part of the dissipation inequality. For the update of the inelastic metric, an elastic predictor-inelastic corrector algorithm is utilized. During inelastic corrector step, an implicit integration scheme is adopted. The resulting nonlinear set of equations are solved iteratively by a Newton

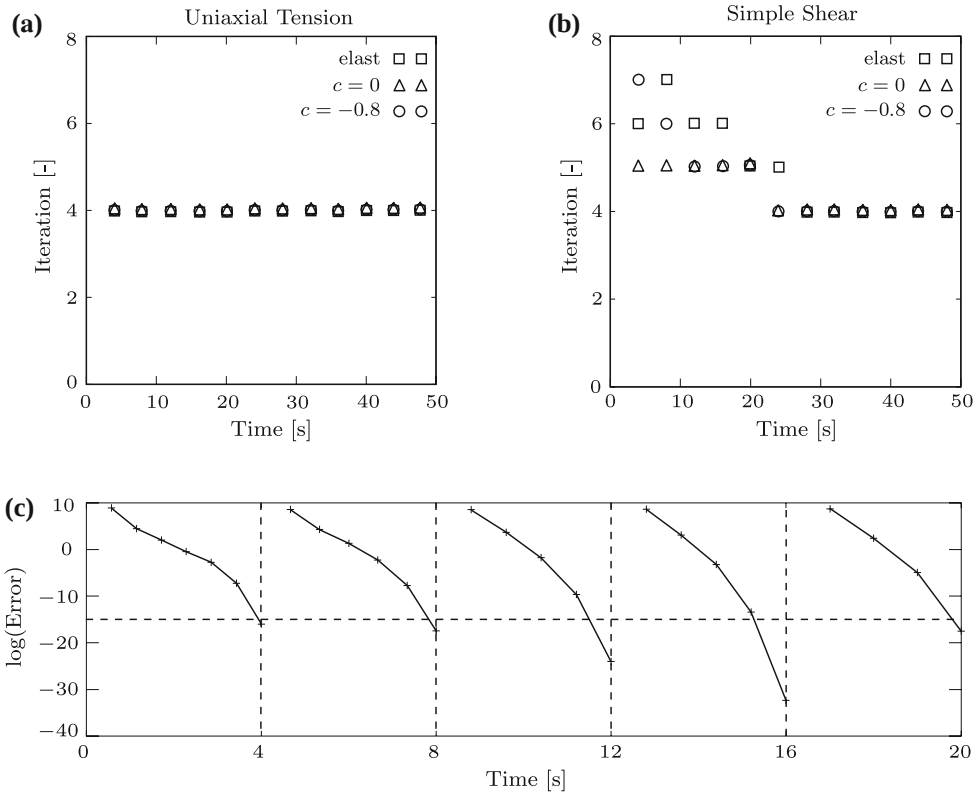

Fig. 12 Number of iterations versus time for **a** uniaxial tension and **b** simple shear simulations in case of ground state elastic reference solution, parameter $c = 0$ and $c = -0.8$, respectively **c** Logarithmic plot of the error (energy norm), evenly distributed within the time increment $\Delta t = 4$ s for the simple shear simulation with $c = -0.8$

iteration. The consistent tangent moduli are computed from a ctitious intermediate stress expression obtained by the pull-back of the Kirchhoff stress to the intermediate con guration by the trial elastic deformation gradient. This scheme is very attractive since it circumvents the rate of the inelastic deformation gradient. Then, the formulation is successfully implemented into FEAP and validated with respect to uniaxial compression data of Bergström and Boyce [1]. The parametric study has been carried out in order to assess the in uence of material parameters on the overall behaviour. The same procedure is repeated for the parameters appearing in the evolution law and their in uence on relaxation curves has been studied. The model is shown to t well with recently published experimental data. The algorithm is validated with a benchmark boundary value problem. Finally, the convergence and stability of the proposed algorithm is elaborated which demonstrates the ef ciency of the algorithmic setting.

Acknowledgments The nancial support of the Deutsche Forschungsgemeinschaft (DFG) under grant Ka 1163/2-1 is gratefully acknowledged.

Appendix A: Volumetric-isochoric split of the deformation gradient and its rates

We begin with the split of $\boldsymbol{F}$ into spherical and unimodular part

$$\boldsymbol{F} = \bar{\boldsymbol{F}}\boldsymbol{F}^{\text{vol}} \tag{A.1}$$

where

$$\bar{\boldsymbol{F}} = J^{-1/3}\boldsymbol{F} \quad \text{and} \quad \boldsymbol{F}^{\text{vol}} = J^{1/3}\boldsymbol{1}. \tag{A.2}$$

Now, consider the spatial velocity gradient $\boldsymbol{l} = \dot{\boldsymbol{F}}\boldsymbol{F}^{-1}$;

$$\begin{aligned}\boldsymbol{l} = \dot{\boldsymbol{F}}\boldsymbol{F}^{-1} &\overset{(A.1)}{=} (\dot{\bar{\boldsymbol{F}}}\boldsymbol{F}^{\text{vol}} + \bar{\boldsymbol{F}}\dot{\boldsymbol{F}}^{\text{vol}})(\boldsymbol{F}^{vol-1}\bar{\boldsymbol{F}}^{-1}) \\ &= \dot{\bar{\boldsymbol{F}}}\bar{\boldsymbol{F}}^{-1} + \bar{\boldsymbol{F}}\dot{\boldsymbol{F}}^{\text{vol}}\boldsymbol{F}^{vol-1}\bar{\boldsymbol{F}}^{-1} \\ &\overset{(A.2)}{=} \dot{\bar{\boldsymbol{F}}}\bar{\boldsymbol{F}}^{-1} + \bar{\boldsymbol{F}}(\tfrac{1}{3}J^{-2/3}\dot{J}\boldsymbol{1}J^{-1/3}\boldsymbol{1})\bar{\boldsymbol{F}}^{-1} \\ &= \dot{\bar{\boldsymbol{F}}}\bar{\boldsymbol{F}}^{-1} + \tfrac{1}{3}\dot{J}J^{-1}\boldsymbol{1} \\ &= \bar{\boldsymbol{l}} + \boldsymbol{l}^{\text{vol}}.\end{aligned} \tag{A.3}$$

We observe that

$$\dot{J} = \partial_{\boldsymbol{F}} J : \dot{\boldsymbol{F}} = J\boldsymbol{F}^{-T} : \dot{\boldsymbol{F}} = J\,\text{tr}\,[\dot{\boldsymbol{F}}\boldsymbol{F}^{-1}] = J\,\text{tr}\,[\boldsymbol{l}]. \tag{A.4}$$

Inserting (A.4) into (A.3), we end up with an additive decomposition of the spatial velocity gradient into volumetric and unimodular contributions

$$\bar{\boldsymbol{l}} = \dot{\bar{\boldsymbol{F}}}\bar{\boldsymbol{F}}^{-1} = \boldsymbol{l} - \tfrac{1}{3}J\,\text{tr}\,[\boldsymbol{l}]\boldsymbol{1} = \boldsymbol{l}^{\text{iso}}. \tag{A.5}$$

Furthermore,

$$\begin{aligned}\boldsymbol{d} &:= \text{sym}(\boldsymbol{g}\boldsymbol{l}) = \text{sym}(\boldsymbol{g}\boldsymbol{l}^{\text{iso}} + \boldsymbol{g}\boldsymbol{l}^{\text{vol}}) \\ &= \text{sym}(\boldsymbol{g}\boldsymbol{l}^{\text{iso}}) + \text{sym}(\boldsymbol{g}\boldsymbol{l}^{\text{vol}}) \\ &= \boldsymbol{d}^{\text{iso}} + \boldsymbol{d}^{\text{vol}}.\end{aligned} \tag{A.6}$$

Therefore, we can rewrite the *Clausius-Planck inequality* in the form

$$\mathscr{D} = [\boldsymbol{\tau}_{\text{vol}} + \boldsymbol{\tau}_{\text{iso}}] : [\boldsymbol{d}^{\text{vol}} + \boldsymbol{d}^{\text{iso}}] - [\dot{U} + \dot{\tilde{\Psi}}] \geq 0. \tag{A.7}$$

Examining that $\boldsymbol{\tau}_{\text{vol}} : \boldsymbol{d}^{\text{iso}} = 0$ and $\boldsymbol{\tau}^{\text{iso}} : \boldsymbol{d}^{\text{vol}} = 0$, (A.7) takes the following form

$$\mathscr{D} = \boldsymbol{\tau}_{\text{vol}} : \boldsymbol{d}^{\text{vol}} + \boldsymbol{\tau}_{\text{iso}} : \boldsymbol{d}^{\text{iso}} - [\dot{U} + \dot{\tilde{\Psi}}] \geq 0. \tag{A.8}$$

We obtain a stronger constraint by decoupling the volumetric and the isochoric parts in the dissipation inequality (A.8) leading to

$$\mathscr{D}_{\text{vol}} = \boldsymbol{\tau}_{\text{vol}} : \boldsymbol{d}^{\text{vol}} - \dot{U} \geq 0 \tag{A.9}$$

and

$$\mathscr{D}_{\text{iso}} = \boldsymbol{\tau}_{\text{iso}} : \boldsymbol{d}^{\text{iso}} - \dot{\tilde{\Psi}} \geq 0. \tag{A.10}$$

Hence, one obtains a discrete representation of the *Clausius-Duhem inequality* for purely isochoric processes of inelasticity.

Appendix B: Derivation of the local tangent for Newton iteration

In this Appendix, the derivation of local tangent $\mathcal{K}_{ab}$ is shown. We recall the residual expression

$$r_a := \varepsilon_a + \frac{\Delta t}{\sqrt{2}} \frac{\dot{\gamma}}{\tau_v} \text{dev}\tau_a - \varepsilon_a^{tr} = 0. \tag{B.1}$$

The local tangent is de ned as

$$\mathcal{K}_{ab} := \left. \frac{\partial r_a}{\partial \varepsilon_b} \right|_{\varepsilon = \varepsilon^k} \tag{B.2}$$

and can be derived from (B.1)

$$\mathcal{K}_{ab} = \delta_{ab} + \frac{\Delta t}{\sqrt{2}} \text{dev}\tau_a \frac{\partial(\dot{\gamma}/\tau_v)}{\partial \varepsilon_b} + \frac{\Delta t}{\sqrt{2}} \frac{\dot{\gamma}}{\tau_v} \frac{\partial \text{dev}\tau_a}{\partial \varepsilon_b}. \tag{B.3}$$

Taking the derivatives in (B.3), one nally obtains the compact definition

$$\boxed{\mathcal{K}_{ab} = \delta_{ab} + \beta_1 \text{dev}\tau_a \mathcal{D}_b + \beta_2 \bar{\mathcal{T}}_{ab},} \tag{B.4}$$

along with the terms de ned below:

$$\beta_1 = \frac{\Delta t}{2\sqrt{2}} (m-1) \frac{\dot{\gamma}_0}{\hat{\tau}^m} (\lambda^i_{\text{chain}})^c \tau_v^{m-3}, \tag{B.5}$$

$$\beta_2 = \frac{\Delta t}{\sqrt{2}} \frac{\dot{\gamma}}{\tau_v}, \tag{B.6}$$

$$\mathcal{D}_b = \sum_{c=1}^{3} \text{dev}\tau_c \mathcal{T}_{cb}, \tag{B.7}$$

$$\bar{\mathcal{T}}_{ab} = \mathcal{T}_{ab} - \frac{1}{3} \sum_{c=1}^{3} \mathcal{T}_{cb}, \tag{B.8}$$

$$\mathcal{T}_{ab} := \frac{\partial \tau_a}{\partial \varepsilon_b} = \frac{2}{3} \mu_v \frac{3 - \lambda_1^{e2}}{1 - \lambda_r^{e2}} \lambda_a \lambda_b \delta_{ab} + \frac{4}{9} \frac{\mu_v}{N_v} \frac{1}{(1 - \lambda_r^{e2})^2} \lambda_a^2 \lambda_b^2. \tag{B.9}$$

References

1. Bergström JS, Boyce MC (1998) Constitutive modeling of the large strain time–dependent behavior of elastomers. J Mech Phys Solids 46:931–954
2. Reese S, Govindjee S (1998) A theory of nite viscoelasticity and numerical aspects. Int J Solids Struct 35:3455–3482
3. Lubliner J (1985) A model of rubber viscoelasticity. Mech Res Commun 12:93–99
4. Simo JC, Miehe C (1992) Associative coupled thermoplasticity at nite strains: formulation, numerical analysis and implementation. ASME J Appl Mech 98:41–104
5. Simo JC (1992) Algorithms for static and dynamic multiplicative plasticity that preserve the classical return mapping schemes of the in nitesimal theory. Comput Methods Appl Mech Eng 99:61–112
6. Weber G, Anand L (1990) Finite deformation constitutive equations and a time integration procedure for isotropic hyperelastic-viscoplastic solids. Comput Methods Appl Mech Eng 79:173–202
7. Cuitino A, Ortiz M (1992) A material-independent method for extending stress update algorithms from small-strain plasticity to nite plasticity with multiplicative kinematics. Eng Comput 9:437–451
8. Ogden R (1972) Large deformation isotropic elastictiy: on the correlation of theory and experiment for incompressible rubberlike solids. Procee R Soc Lond A 326:565–584
9. Areias P, Matous K (2008) Finite element formulation for modeling nonlinear viscoelastic elastomers. Comput Methods Appl Mech Eng 197:4702–4717
10. Marckmann G, Verron E (2006) Comparion of hyperelastic models for rubber-like materials. Rubber Chem Technol 12:835–858
11. Treloar LRG (1944) Stress–strain data for vulcanised rubber under various types of deformation. Trans Faraday Soc 40:59–70
12. Kawabata S, Matsuda M, Tei K, Kawai H (1998) Experimental survey of the strain energy density function of isoprene rubber vulcanizate. Macromolecules 14:154–162
13. Kaliske M, Heinrich G (1998) An extended tube–model for rubber elasticity: statistical–mechanical theory and nite element implementation. Rubber Chem Technol 72:602–632
14. Miehe C, Göktepe S, Lulei F (2004) A micro–macro approach to rubber–like materials. Part I: The non–af ne micro–sphere model of rubber elasticity. J Mech Phys Solids 52:2617–2660
15. Arruda EM, Boyce MC (1993) A three–dimensional constitutive model for the large stretch behavior of rubber elastic materials. J Mech Phys Solids 41:389–412
16. Green MS, Tobolsky AV (1946) A new approach to the theory of relaxing polymeric media. J Chem Phys 14:80–92
17. Lodge AS (1956) A netowork theory of ow birefringence and stress in concentrated polymer solutions. Trans Faraday Soc 52:120–130
18. Phan-Thien N (1978) A nonlinear network viscoelastic model. J Rheol 22:259–283
19. Tanaka F, Edwards SF (1992) Viscoelastic properties of physically crosslinked networks. I: Non–linear stationary viscoelasticity. J Non-Newtonian Fluid Mech 43:247–271
20. Tanaka F, Edwards SF (1992) Viscoelastic properties of physically crosslinked networks. II: Dynamic mechanical moduli. J Non-Newtonian Fluid Mech 43:289–309

21. de Gennes PG (1971) Reptation of a polymer chain in the presence of xed obstacles. J Chem Phys 55:572–579
22. Doi M, Edwards SF (1986) The theory of polymer dynamics. Clarendon Press, Oxford
23. Miehe C, Göktepe S (2005) A micro–macro approach to rubber-like materials. Part II: The micro–sphere model of nite rubber viscoelasticity. J Mech Phys Solids 53:2231–2258
24. Miehe C (1998) A constitutive frame of elastoplasticity at large strains based on the notion of a plastic metric. Int J Solids Struct 35:3859–3897
25. Amin AFMS, Lion A, Sekita S, Okui Y (2006) Nonlinear dependence of viscosity in modeling the rate-dependent response of natural and high damping rubbers in compression and shear: Experimental identi cation and numerical veri cation. Int J Plast 22:1610–1657
26. Cohen A (1991) A Padé approximant to the inverse langevin function. Rheol Acta 30:270–273
27. Diani J, Gilormini P (2005) Combining the logarithmic strain and the full-network model for a better understanding of the hyperelastic behaviour of rubber-like materials. J Mech Phys Solids 53:2579–2596
28. Simo JC, Taylor RL, Pister KS (1985) Variational and projection methods for the volume constraint in nite deformation elasto–plasticity. Comput Methods Appl Mech Eng 51:177–208
29. Miehe C (1994) Aspects of the formulation and nite element implementation of large strain isotropic elasticity. Int J Numer Methods Eng 37:1981–2004
30. Bergström JS, Boyce MC (2001) Constitutive modeling of the time-dependent and cyclic loading of elastomers and application to soft biological tissues. Mech Mater 33:523–530
31. Huber N, Tsakmakis C (2000) Finite deformation viscoelasticity laws. Mech Mater 32:1–18